Subradiance-enhanced excitation transfer between dipole-coupled nanorings of quantum emitters

Maria Moreno-Cardoner,[1,2] David Plankensteiner,[3] Laurin Ostermann,[3] Darrick E. Chang,[1,4] and Helmut Ritsch[3]
[1]*Institut de Ciencies Fotoniques, The Barcelona Institute of Science and Technology, 08860 Castelldefels, Barcelona, Spain*
[2]*Física Teòrica: Informació i Fenòmens Quàntics, Departament de Física, Universitat Autònoma de Barcelona, 08193 Bellaterra, Spain*
[3]*Institut für Theoretische Physik, Universität Innsbruck, Technikerstrasse 21a, A-6020 Innsbruck, Austria*
[4]*Institució Catalana de Recerca i Estudis Avançats, 08015 Barcelona, Spain*

(Received 20 February 2019; revised manuscript received 27 May 2019; published 7 August 2019)

A ring of dipole-coupled quantum emitters positioned at subwavelength distances possesses only a few radiant but many subradiant collective excitations with lifetimes growing exponentially with the atom number. These exhibit a three-dimensionally confined spatial radiation field pattern and form nanoscale high-Q optical resonators. Tailoring size, orientation, and distance between two rings allows for increasing the ratio of coherent ring-to-ring energy transfer versus free-space emission by orders of magnitude. In particular, the more dark and delocalized over several sites are excitons, the higher is their fidelity for transport to a second ring.

DOI: 10.1103/PhysRevA.100.023806

I. INTRODUCTION

Identifying efficient mechanisms for radiant energy transfer between designated subsystems without loss to the environment is a key ingredient in many physical applications including solar energy conversion, photosynthetic processes, and, in particular, coherent-state transfer in optical quantum communication. In quantum information processing and communication optical fibers are a viable solution for transporting photonic bits with minimal loss. Via an evanescent field overlap light can be coupled in and out of such structures. Waveguides closed to a loop form optical ring resonators with applications as switches, high-order optical filters, and optomechanical sensors.

Spontaneous emission from a single atom in free space is strongly modified by dipole-dipole interactions with identical emitters close by, leading to fast decay via super-radiant states or long-lived subradiant behavior [1–8]. Surprisingly, as one consequence of strong dipole-dipole coupling, a chain of subwavelength spaced quantum emitters acts like an ideal optical waveguide transporting excitation energy with minimal dissipation [9–12]. Excitons with wave vectors surpassing the free-space photon wave vector become perfectly dark for infinitely extended chains [9,10]. As photon emission occurs at its ends only, even for a finite chain of emitters the excited-state lifetime still grows with the third power of the atom number [8,10,13,14]. Low-loss guiding studies have also been performed for chains of gold nanoparticles [15]. However, in contrast to conventional fibers such atom chains constitute active optical devices which can, e.g., be employed for efficient optical photon storage [10].

The central phenomenon studied here is resonant excitation transfer between two separate dipole arrays. We focus on the specific example of regular rings, which, as we show in the following, have extraordinary radiative properties [10] with intriguing field distributions. Each ring of dipoles implements a minimalist form of an optical ring resonator as depicted in Fig. 1, which can exchange energy with a second ring close by. Although the strong transverse field confinement of subradiant states leads to an exponential field decay with distance, energy is still transferred between rings with almost negligible loss [11].

As with conventional fiber-optical ring resonators two such rings are coupled via their field mode overlap which should be large compared to free-space decay. Efficient coherent coupling between two long-lived states is a central ingredient required for distributed quantum computing [16]. We find that subradiant states of individual rings feature a slower but much more efficient ring-to-ring energy transfer than super-radiant states.

Note that many light-harvesting complexes such as LHC-II in biological systems exhibit a structure of coupled dipole rings [17–20]. While modeling these molecules realistically certainly requires a much more detailed and sophisticated description, a corresponding simplistic model of outer dipole rings commonly coupled to a central inner ring [21] shows a wealth of complex, nontrivial dynamics with evidence of coherent excitation propagation [21,22] or an enhanced optical absorption [20] already. In our toy model inspired by this geometry, dark states play an essential role in the coupled dynamics and energy transfer between the rings.

II. SYSTEM

Let us consider N identical two-level quantum emitters with given dipole orientations (denoted by $\hat{\boldsymbol{\wp}}_j$, $j = 1, \ldots, N$) positioned in a regular polygon with interparticle distance d [see Fig. 1(a)], which possess a single narrow optical resonance around a frequency ω_0. Integrating over the electromagnetic degrees of freedom in the Born-Markov approximation [1] leads to the dynamics of the atomic excitations governed by the master equation $\dot{\rho} = -(i/\hbar)[H, \rho] + \mathcal{L}[\rho]$ (from now on $\hbar = 1$). The Hamiltonian in a frame rotating at ω_0 reads

$$H = \sum_{ij;i\neq j} \Omega_{ij} \sigma_i^{eg} \sigma_j^{ge}, \tag{1}$$

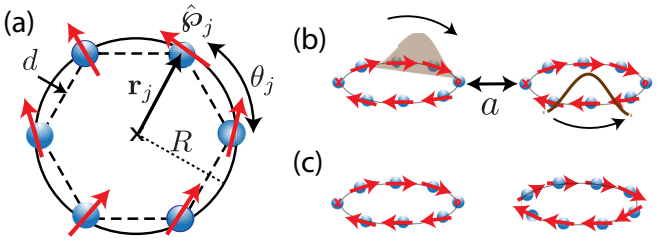

FIG. 1. Scheme of the system. (a) A single ring with interparticle distance d, radius R, and angular position given by $\theta_j = 2\pi(j-1)/N$. The red arrows show the dipoles' (arbitrary) orientations $\hat{\boldsymbol{\wp}}_j$. (b, c) A single wave-packet excitation is transferred between two in-plane rings separated by the distance a. Panels (b) and (c) correspond to the site-site and site-edge configurations for tangential dipoles, respectively.

where $\sigma_j^{ge} = |g_j\rangle\langle e_j|$ is the atomic lowering operator between the excited and ground states of atom j, and $\sigma_j^{eg} = (\sigma_j^{ge})^\dagger$. The Lindblad operator is

$$\mathcal{L}[\rho] = \frac{1}{2}\sum_{i,j}\Gamma_{ij}\left(2\sigma_j^{ge}\rho\sigma_i^{eg} - \sigma_i^{eg}\sigma_j^{ge}\rho - \rho\sigma_i^{eg}\sigma_j^{ge}\right). \quad (2)$$

The dipole interaction and collective decay matrices with elements Ω_{ij} and Γ_{ij}, respectively, are given by

$$\Omega_{ij} = -\frac{3\pi\Gamma_0}{k_0}\hat{\boldsymbol{\wp}}_i^* \cdot \mathrm{Re}\boldsymbol{G}(\vec{r}_i - \vec{r}_j, \omega_0)\cdot\hat{\boldsymbol{\wp}}_j, \quad (3)$$

$$\Gamma_{ij} = \frac{6\pi\Gamma_0}{k_0}\hat{\boldsymbol{\wp}}_i^* \cdot \mathrm{Im}\boldsymbol{G}(\vec{r}_i - \vec{r}_j, \omega_0)\cdot\hat{\boldsymbol{\wp}}_j, \quad (4)$$

where $\boldsymbol{G}(\boldsymbol{r}, \omega_0)$ is the Green's tensor in free space, which acts on an oscillating unit dipole according to

$$\boldsymbol{G}(\boldsymbol{r}, \omega_0)\cdot\hat{\boldsymbol{\wp}} = \frac{e^{ik_0 r}}{4\pi r}\Bigg[(\hat{\mathbf{r}}\times\hat{\boldsymbol{\wp}})\times\hat{\mathbf{r}} + \left(\frac{1}{k_0^2 r^2} - \frac{i}{k_0 r}\right)[3\hat{\mathbf{r}}(\hat{\mathbf{r}}\cdot\hat{\boldsymbol{\wp}}) - \hat{\boldsymbol{\wp}}]\Bigg]. \quad (5)$$

Here, $\hat{\mathbf{r}} = \boldsymbol{r}/|\boldsymbol{r}|$ is the position unit vector, $k_0 = \omega_0/c$ is the wave number associated with the atomic transition, and $\Gamma_0 = |\boldsymbol{\wp}|^2 k_0^3/3\pi\epsilon_0$ is the spontaneous emission rate of a single emitter with dipole moment strength $|\boldsymbol{\wp}|$.

After solving for the atomic density matrix, the EM fields can be obtained from a generalized input-output relation [10,23], which in the absence of an external field reads

$$\boldsymbol{E}^+(\boldsymbol{r}) = \frac{|\boldsymbol{\wp}|k_0^2}{\epsilon_0}\sum_i \boldsymbol{G}(\boldsymbol{r} - \boldsymbol{r}_i, \omega_0)\cdot\hat{\boldsymbol{\wp}}_i\sigma_i^{ge}. \quad (6)$$

In the following we will restrict ourselves to the single-excitation manifold so that for the observables of interest (such as the fields generated by the ring or the excited-state population) we can neglect the recycling term (first term in the Lindblad expression). This term accounts for the change in the ground-state population only. The system's properties can then be fully understood via the eigenstates of an effective non-Hermitian Hamiltonian:

$$H_{\mathrm{eff}} = \sum_{ij}\left(\Omega_{ij} - i\frac{\Gamma_{ij}}{2}\right)\sigma_i^{eg}\sigma_j^{ge} \quad (7)$$

with $\Omega_{ii} = 0$.

III. RADIATIVE PROPERTIES OF A SINGLE RING

As discussed in [8,10] dipole-dipole interactions dramatically modify the collective decay of an ordered array of dipoles. The eigenstates of H_{eff} define a set of collective modes with associated complex eigenvalues, the real and imaginary parts of which correspond to the collective frequency shifts and decay rates. For a symmetric ring configuration where the dipole orientations preserve the rotational symmetry, e.g., if the dipoles are oriented perpendicularly to the plane of the ring, or tangentially along the ring, the collective modes in the single-excitation manifold are perfect spin waves with well-defined angular momenta, which can be written as $|\psi_m\rangle = \tilde{\sigma}_m^{eg}|g\rangle$, with

$$\tilde{\sigma}_m^{eg} = \frac{1}{\sqrt{N}}\sum_{j=1}^{N} e^{im\theta_j}\sigma_j^{eg}. \quad (8)$$

Here, $\theta_j = 2\pi(j-1)/N$ is the angular coordinate of site j and $m = 0, \pm1, \pm2, \cdots, \lceil\pm(N-1)/2\rceil$ is the (integer) angular momentum of the mode. In these states the single excitation is completely delocalized over all sites, and its angular momentum is well defined. The corresponding eigenvalues are given by

$$\lambda_m = \frac{1}{N}\sum_{j\ell} e^{im(\theta_\ell - \theta_j)}\left(\Omega_{j\ell} - i\frac{\Gamma_{j\ell}}{2}\right). \quad (9)$$

Note that, due to the rotational symmetry, the coupling is invariant under a translation along the ring, i.e., $\Omega_{j\ell} = \Omega_{j+1\ell+1}$ (and equivalently for $\Gamma_{j\ell}$). The real and imaginary parts of these eigenvalues define the collective frequency shifts and emission rates of the mode $J_m = \mathrm{Re}\{\lambda_m\}$ and $\Gamma_m = -2\mathrm{Im}\{\lambda_m\}$, respectively. It is easy to see that the spectrum will be symmetric under the exchange $m \leftrightarrow -m$, that is, $\lambda_m = \lambda_{-m}$. We note that the mode $m = 0$ is always nondegenerate, whereas the eigenstates with a maximum value of m will be doubly degenerate if N is odd.

As we decrease the interparticle distance d with respect to the light's wavelength $\lambda = 2\pi/k_0$, we expect to approach the Dicke limit [24]. In this limit the emitters are so close that the range of the interaction is effectively infinite, yielding a single bright mode decaying at rate $N\Gamma_0$, and $N-1$ perfectly dark modes. This happens for the case of dipoles transversally oriented to the ring, as it is shown in Fig. 2(a), where we have plotted the collective decay rates as a function of the decreasing particle separation. For tangential polarization, instead, there are two bright modes corresponding to $m = \pm1$ with a decay rate $N\Gamma_0/2$, while $m = 0$ is dark by symmetry, as shown in Fig. 2(b).

We observe the linear scaling of the decay of the most radiant mode with the number of emitters by gradually increasing the density of emitters in the ring, while keeping its radius constant. This is shown in Fig. 2(c) for transverse polarization. In addition, the covered frequency spectrum becomes larger as the ring gets denser. The polarization orientation will determine whether the dark or bright modes are lower or higher in energy. For instance, for transverse polarization, bright modes are lower in energy, whereas for tangential polarization (closer to a head-tail configuration of the dipoles) bright modes are higher in energy.

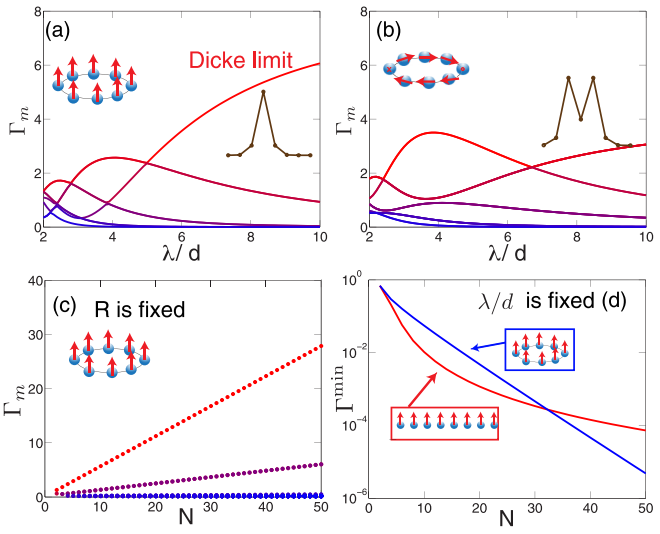

FIG. 2. Single ring radiative properties. (a) Collective decay rates Γ_m (in units of Γ_0) as a function of λ/d, for a ring of $N = 8$ emitters with transverse polarization and a single excitation. In the Dicke limit, $\lambda/d \to \infty$, only a single bright mode with a decay rate on the order of $N\Gamma_0$ is present, and $N - 1$ modes are dark. (b) Identical setup as in panel (a) but for tangential polarization. Two bright modes arise in the Dicke limit at $m = \pm 1$. (c) Γ_m (in units of Γ_0) for a ring of fixed radius $R = 0.15\lambda$ with transverse polarization, when increasing the density of emitters. For the bright mode, $\Gamma \sim N\Gamma_0$. (d) Decay rate (log scale) of the most subradiant eigenmode vs the atom number, for a ring (blue circles) and an open linear chain (red circles), both with $\lambda = 3d$. The lifetime of the most subradiant mode in the ring increases exponentially with the atom number.

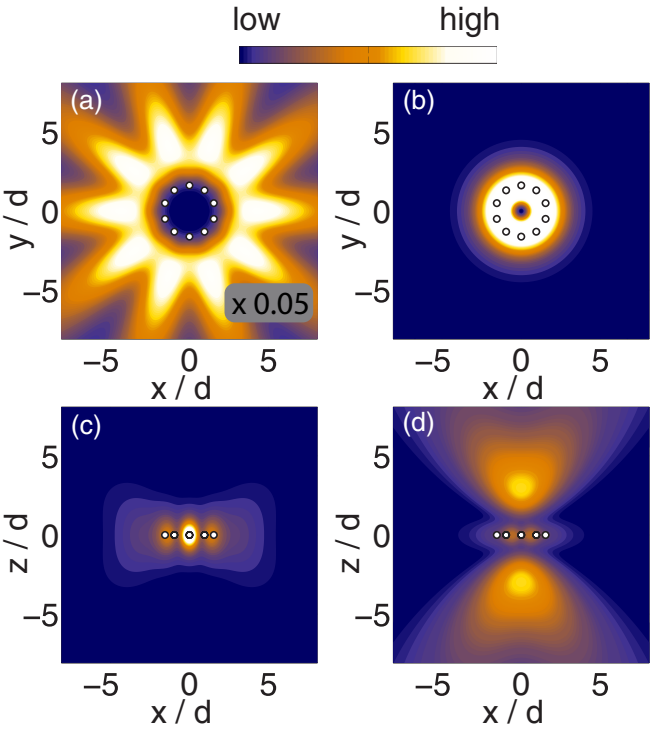

FIG. 3. Single ring radiation patterns. The field intensity of a single excitation in a ring with tangential polarization (a, c) in the most subradiant mode with $m = N/2$ (N even) and (b, d) in the radiant mode with $m = 0$. The top panels (a, b) show the field in the xy plane at fixed $z = 1.5R$. The bottom panels (c, d) show the field in the xz plane at fixed $y = 1.5R$. The white circles represent the positions of the emitters. The field pattern for the subradiant mode concentrates outside the ring while it vanishes at the center of the ring, whereas the radiant field is confined to a subwavelength region in the center ($N = 10$, $d/\lambda = 0.4$).

Moreover, the modes of the ring feature extraordinary radiative properties in contrast to an open linear chain. For a growing number of emitters strongly subradiant modes with exponentially growing lifetimes appear. If we increase the number of emitters while keeping λ/d constant, the system will start to locally resemble an infinite chain studied in detail in [10]. Interestingly, dark modes in an infinite chain correspond to spin waves characterized by a wave number larger than k_0. In this case the eigenmode generates an exponentially decaying evanescent field transverse to the chain and therefore the emitters can guide light perfectly, just like an optical fiber. For a finite chain, these modes retain a small decay rate since a photon can still scatter off the ends of the chain. However, by bending and closing the chain to a ring, the excitation lifetime is drastically increased. For a sufficiently large ring this approaches an exponential suppression of the decay rate with the number of emitters [10]. This is in contrast to the polynomial suppression ($\sim N^{-3}$) observed for an open linear chain. A comparison of how the smallest decay rate scales with the atom number in the two cases is shown in Fig. 2(d).

A closer look at the electromagnetic fields generated by super-radiant or subradiant eigenmodes of a ring by means of Eq. (6) reveals radically different properties. In Fig. 3 the fields of the most subradiant eigenmode (left column) and a super-radiant eigenmode (right column) for a ring with tangential polarization exhibit remarkably distinct radiation patterns. In the case of a subradiant mode the field is evanescent (nonpropagating) transverse to the plane that contains the ring and vanishes at the center of the ring. The radiant state, on the other hand, causes strong dipolar emission and shows a tightly confined maximum at the center of the ring.

IV. TAILORED COLLECTIVE COUPLING OF TWO RINGS

We continue with the study of two coupled rings which lie in the same plane and are separated by a distance a [see Figs. 1(b) and 1(c)]. In particular, we study how excitations are transferred from one ring to another with minimal loss. While super-radiant states possess the strongest dipole moments and thus couple strongly to neighboring dipoles, they also feature a much faster decay.

A. Coupled rings radiation patterns

As a first step we look at the fields radiated by two rings in close proximity: it was previously shown that the eigenstates of the effective Hamiltonian and the corresponding field distributions inherit the angular symmetry of the dipole rings. However, this is modified for two rings when their radiated fields overlap. We choose the states of each ring as an eigenstate characterized by its angular momentum $m_{1,2}$ as defined in Eq. (8). The total state of the two rings is then given

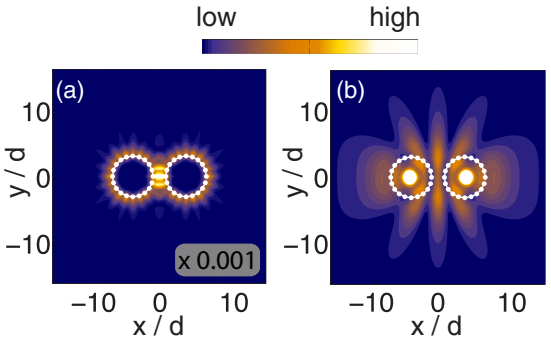

FIG. 4. Coupled rings radiation patterns. The two rings are (a) in the most subradiant mode ($m_1 = m_2 = N/2$) and (b) in a radiant mode ($m_1 = m_2 = 0$). The white circles represent the positions of the dipoles. The dipole orientation is transverse to the plane containing the rings ($N = 20$, $d/\lambda = 0.25$, $a = 2d$, $z = \lambda/2$).

by a symmetric superposition of the two and we compute the field using Eq. (6). Dark and bright states again show very distinct field distributions. In Fig. 4 we compare the radiated fields when the two rings are in the most subradiant state, i.e., $m_1 = m_2 = \lceil (N-1)/2 \rceil$ [Fig. 4(a)], and when the two rings are in a radiant state $m_1 = m_2 = 0$ [Fig. 4(b)]. In the subradiant case, the field concentrates at the contact region between the two rings. Overall, the field radiated by the subradiant rings is very weak. These two facts already indicate that subradiant states offer efficient transport of excitations since they preferentially radiate from one ring to the other with small losses. Super-radiant states, however, exhibit large decay into the center of each ring as well as to the sides. We can thus expect that losses via spontaneous emission will dominate.

B. Ring-to-ring coupling

In order to support these intuitive findings, we proceed by quantifying the dispersive as well as the dissipative coupling between the rings. To this end, consider that the terms in the effective Hamiltonian [Eq. (7)] corresponding to the coupling between the two rings can be written in the angular momentum basis as

$$H_{\text{eff}}^{1,2} = \sum_{m_1,m_2} \left(J_{m_1,m_2} - i\frac{\Gamma_{m_1,m_2}}{2} \right) \tilde{\sigma}^{eg}_{m_1,1} \tilde{\sigma}^{ge}_{m_2,2}. \tag{10}$$

Here, $J_{m_1,m_2} = \text{Re}\{\lambda_{m_1,m_2}\}$ is the dispersive coupling and $\Gamma_{m_1,m_2} = -2\text{Im}\{\lambda_{m_1,m_2}\}$ is the dissipative coupling, and

$$\lambda_{m_1,m_2} = \frac{1}{N} \sum_{\substack{i \in \mathcal{R}_1, \\ j \in \mathcal{R}_2}} \left(\Omega_{ij} - i\frac{\Gamma_{ij}}{2} \right) e^{i(m_1\theta_i - m_2\theta_j)}. \tag{11}$$

As a shorthand notation, we have defined two sets of indices, one for the sites in the first ring, $\mathcal{R}_1 = \{1, 2, \ldots, N\}$, and one for the sites in the second ring, $\mathcal{R}_2 = \{N+1, \ldots, 2N\}$.

In Figs. 5(a) and 5(b), we show the dispersive and dissipative couplings as a function of the angular momentum of the two rings m_1 and m_2. We use the configuration shown in Fig. 1(b) with a fixed separation between the two rings $a = 0.15\lambda$ and tangential polarization. The white dashed line

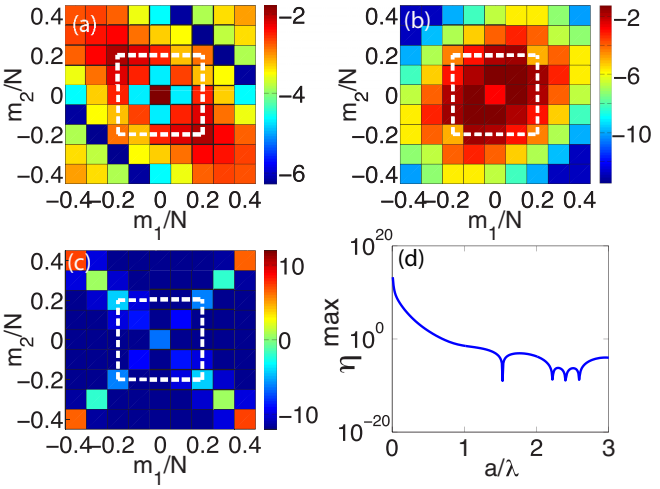

FIG. 5. Ring-to-ring coupling. (a) Absolute value of the dispersive (J_{m_1,m_2}) coupling. (b) Absolute value of the dissipative (Γ_{m_1,m_2}) coupling. (c) Ratio η_{m_1,m_2} on a logarithmic scale for spin-wave states with angular momenta m_1 and m_2. The rings lie in the same plane separated by $a = 0.15\lambda$ as shown in Fig. 1(b). The dashed white line denotes the light line (free-space wave vector) beyond which the modes are mainly subradiant. Subradiant states primarily couple to subradiant states. Moreover, η is maximal for pairs of subradiant states with opposite angular momenta. (d) The maximum value of η_{m_1,m_2} obtained with $m_1 = m_2 = N/2$, as a function of the ring separation a ($N = 10$, $d/\lambda = 0.1$).

in Figs. 5(a)–5(c) encloses the region where states are predominantly radiant, such that $2\pi m/N < k_0 d$ for both $m = m_1$ and m_2. Physically, this corresponds to the light line, or states generating fields that follow the dispersion relation of light in vacuum propagating along a very large ring, for which the curvature is negligible. We observe that subradiant states mainly couple dispersively to other subradiant states, whereas radiant states couple to other radiant states with a large dissipation. In Fig. 5(c) we show, as a figure of merit that quantifies how efficiently two modes in the two rings are coupled (and thus how efficiently an excitation can be transferred between them), the ratio

$$\eta_{m_1,m_2} \equiv \frac{J^2_{m_1,m_2}}{4\Delta^2_{m_1,m_2} + (\Gamma_{m_1} + \Gamma_{m_2} + \Gamma_{m_1,m_2})^2}, \tag{12}$$

with $\Delta_{m_1,m_2} = |J_{m_1} - J_{m_2}|$. Remarkably, we find that in the subradiant sector η is non-negligible for states where $m_1 = \pm m_2$ only. Moreover, we find that it is several orders of magnitude larger for $m_1 = -m_2$, that is, for two guided modes that propagate in opposite directions in the two rings. This result indicates that in the subradiant regime the physics is well captured by a two-mode model consisting of the two states with m and $-m$.

We also note that the efficiency in the coupling strongly depends on the particular configuration of the dipoles. As the separation between the rings increases, the maximum value of η displays oscillations with an overall decay. This is shown in Fig. 5(d), where we have evaluated $\eta^{\max} = \eta_{m_1=N/2,m_2=N/2}$ for $N = 10$ as a function of the rings' separation a. Interestingly, a different configuration such as the site-edge arrangement

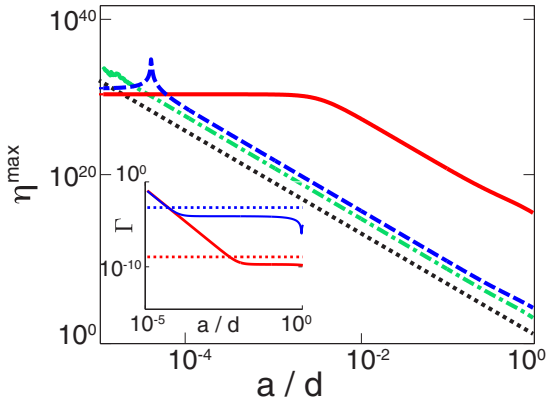

FIG. 6. Scaling of the ratio between dispersive and dissipative couplings with the rings' separation. The parameter $\eta^{\max} = \eta_{N/2,N/2}$ is plotted for two coupled rings with $d/\lambda = 0.1$ and tangential polarization, as a function of the rings' separation a. The dashed blue and solid red lines are for $N = 10$ and 20, respectively. For comparison, we plot the same quantity for two coupled linear chains with $N = 20$ and tangential polarization (dot-dashed green line) and the squared ratio between dispersive and dissipative emission for the case of two coupled single atoms (dotted black line), separated by the distance a. In both cases the ratio scales with distance as $\sim 1/k_0^3 a^3$, in stark contrast to the coupled rings case, for which it saturates at short distances. The inset shows the dissipative coupling (solid lines) and single ring decay rate (dotted lines) for the two coupled rings and the cases $N = 10$ (blue upper lines) and 20 (red lower lines). All plots are shown in a log-log scale.

illustrated in Fig. 1(c) can lead to a dramatically different result. In this case, we see that due to the symmetry the fields created by the two rings in the $m = N/2$ mode interfere completely destructively, resulting in a coupling which is exactly zero.

C. Scaling of couplings with the rings' separation

Finally, we conclude this section by discussing a feature that makes the coupled rings geometry unique. For two coupled rings prepared in a subradiant state, the ratio between dispersive and dissipative couplings saturates to a constant value when decreasing the distance between them, in stark contrast to the case of two coupled single atoms or two coupled linear atomic chains.

For two single atoms separated by the distance a that are polarized perpendicularly with respect to the line that connects them, the ratio between dispersive and dissipative couplings scales at short distances as $\approx 3\Gamma_0/4k_0^3a^3$ ($\approx -3\Gamma_0/2k_0^3a^3$ if the polarization is parallel instead). For two atomic arrays prepared in the most subradiant state $m = N/2$ (N even), the squared ratio is directly given by $\eta^{\max}$ (the total dissipative emission is taken as $2\Gamma_m + \Gamma_{m,m}$).

As shown in Fig. 6, $\eta^{\max}$ saturates to a constant value at short enough distances, in contrast to the ratio for two coupled single atoms, which continuously decreases when increasing their distance. The special behavior for the coupled rings is due to the exponential suppression of the single ring decay, which at short enough distances becomes smaller than the inter-ring dissipative coupling, as shown in the inset of the same figure. In this region the total dissipation is dominated by the dissipative coupling, which scales with distance in the same way as the dispersive coupling, thus leading to a constant value of the ratio. In the same figure, we show that this is not the case for two coupled linear chains, which follow the same scaling as the two coupled single atoms.

V. EFFICIENT EXCITATION TRANSFER BETWEEN TWO RINGS

According to the above results for coupling and decay one can expect that for a subradiant excitation in one ring the energy oscillates between the two rings for a very long time before it finally decays. This relates to eigenstates of the system, which are fully delocalized in one ring as opposed to looking at single excited sites.

We proceed by investigating the energy transport efficiency between two rings, as a function of the degree of localization of the initial wave packet. We consider a partially localized wave packet initially prepared in the form

$$\left|\Psi_{i,k}^{\nu}\right\rangle = \frac{1}{\sqrt{n}} \sum_{j\in\mathcal{R}_i} e^{i\nu\theta_j} e^{-\frac{|r_j - r_k|^2}{2\sigma^2}} \sigma_j^{eg} |g\rangle \,, \tag{13}$$

with $\sigma^2 = R^2\Delta\theta^2$. This corresponds to a Gaussian population distribution centered at site k in the ith ring with an angular spread $\Delta\theta$ (wave-packet width $R\cdot\Delta\theta$) and central momentum ν. The constant n accounts for the normalization. A completely delocalized wave packet of this form represents the eigenstate given by ν while a wave packet with zero spread amounts to the atom at the site k being excited only.

For a mode guided by the first ring with momentum m, it is only natural that it will invert its direction upon being transported to the second ring. This is a more intuitive picture of the previous result that the coupling is optimal between modes with opposite m. Thus, for a finite width wave packet, we expect that it is transferred into a wave packet with the same shape but central momentum $-m$. Therefore, we evaluate the fidelity $\mathcal{F}(t)$ of transferring this wave packet to the second ring as

$$\mathcal{F}(t) = \max_k \left\{ \left| \left\langle \Psi_{2,k}^{\nu} \middle| \Psi(t) \right\rangle \right|^2 \right\}, \tag{14}$$

with $\nu = -m$ and where we maximize over the site index k in the second ring since we do not know the (center) position of the wave packet created there at all times. The wave function $|\Psi(t)\rangle$ is given by the time evolution with H_{eff} with the initial condition $|\Psi(0)\rangle = |\Psi_{1,k'}^{m}\rangle$, and k' as indicated later.

In Fig. 7(a) we show the maximal fidelity during the time evolution as a function of the ring separation as well as of the width of the initial wave packet for two rings with $N = 20$. We start out with a wave packet centered at the site that is farthest from the second ring, i.e., $k' = \lfloor N/2 \rfloor$. The momentum is chosen to be $m = \lfloor N/4 \rfloor$ such that all modes the packet is made up of have momenta of the same sign. As one can see, the fidelity is rather low as long as the width is small, i.e., the excitation is localized at one site almost perfectly. However, for a comparably small width in real space, the wave packet is sufficiently localized in momentum space in order to exhibit coherent transport. The fidelity grows to values larger than 90% quickly as the width increases, indicating a reliable

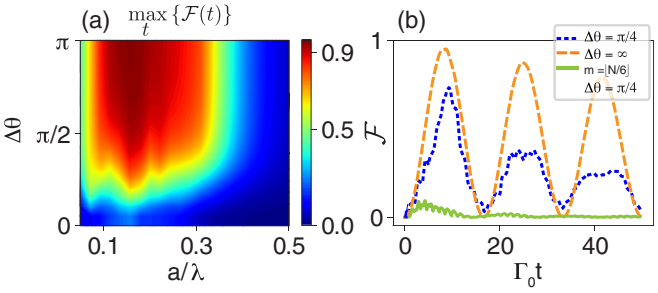

FIG. 7. Fidelity of wave-packet transport between two rings. (a) A scan of the maximal fidelity (over time) as a function of the ring separation and the wave-packet width for two rings of $N = 20$ atoms. For a sufficiently large wave-packet size and a separation comparable to the interparticle distance $d = 0.1\lambda$, the transfer fidelity is almost unity. (b) The larger the width in real space and the localization in momentum space the better the transport. The separation between the rings is $a = 0.15\lambda$. For both panels (a) and (b) the dipoles are oriented tangentially.

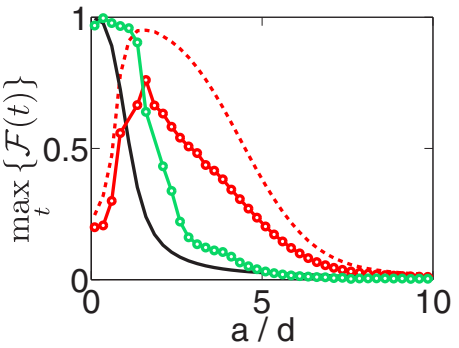

FIG. 8. Comparison of the maximum fidelity of wave-packet transport for different array geometries. The maximum fidelity over time is plotted for two coupled rings with $N = 20$ (red circles), two coupled linear chains with $N = 20$ (green circles), and two coupled single atoms (black line), as a function of separation distance a. The dashed red line is the result for the transport of a subradiant spin wave with angular momentum equal to the central one of the wave packet. The polarization is chosen to be tangential, and $d/\lambda = 0.1$ for the atomic arrays.

transport of a subradiant wave packet from the first ring to the next. Additionally, the transport is best if the separation between the rings is comparable to the interparticle distance. This is due to the change of the energetic shifts of neighboring atoms with their separation: if the atoms at the points where the rings are closest are too far from (or too close to) one another, the shifts vary greatly, effectively detuning these atoms from the rest. Excitations can then no longer propagate.

In Fig. 7(b) we plot the fidelity of the same wave packet being transported as a function of time. The wave packet oscillates between the two rings with the same period for both finite and infinite width. The amplitude, however, damps out considerably faster for the case of a finite width. Nevertheless, a large fidelity is achieved even if the initial state is not a perfect eigenstate of the system. For comparison, we show in the same plot the result for an identical wave packet but with a momentum of $m = \lfloor N/6 \rfloor$, which lies close to the light line and corresponds to a radiant state.

For completeness, we also compare the previous result with $m = \lfloor N/4 \rfloor$ and $\Delta\theta = \pi/4$, with the transport fidelity between two single atoms and two coupled linear atomic chains. For two single atoms, the initial state corresponds to the first atom excited, i.e., $|\Psi(t=0)\rangle = \sigma_1^{eg}|g\rangle$. For the two coupled linear chains, we consider again the wave packet given by Eq. (13) with the same central momentum, $k' = \lfloor N/4 \rfloor$ and $\sigma = N/4$, and evaluate the fidelity from Eq. (14) with $\nu = m$. The maximum fidelity in time for the three cases is shown in Fig. 8, as a function of the distance a between rings, chains, or atoms. This plot clearly shows that for distances $a \gtrsim d$ the fidelity is largest for the case of two coupled rings.

VI. CONCLUSIONS

We have shown that the peculiar radiative properties of excitons in a single ring of dipole coupled emitters lead to special field distributions resembling a circular waveguide field for a subradiant state and a tightly confined intensity for a super-radiant state.

Consequently for another ring in its vicinity optimal coherent coupling occurs between subradiant states of each ring. An excitation that is sufficiently delocalized and moving with a velocity along one ring that closely corresponds to the momentum of an eigenstate that is subradiant can be transported to another ring with a large fidelity. This reliable coherent transport takes place for a comparably small delocalization already and culminates in damped Rabi-like oscillations between the rings once the excitation is spread over the entire first ring.

Note that beyond the two-level approximation analogous bright and dark states also appear in more complex level structures with several decay channels [25]. Hence much of the physics discussed here should also hold in rings of particles with a more complex internal structure.

Note added. Recently, we became aware of related work on coupling between two planar arrays using collective dark states [26].

ACKNOWLEDGMENTS

We acknowledge financial support from the Austrian Science Fund through Project No. P29318-N27 (H.R. and L.O.) and within the Innsbruck Doctoral School DK-ALM Project No. W1259-N27 (D.P.) as well as from European Research Council starting grant FOQAL, MINECO Plan Nacional CANS grant, MINECO Severo Ochoa Grant No. SEV 2015-0522, CERCA Programme/Generalitat de Catalunya, AGAUR Grant No. 2017-SGR-1334, Fundacio Privada Cellex (D.C.), MINECO Grant No. FIS2016-80681-P, and the Generalitat de Catalunya, AGAUR Grant No. 2017-SGR-1127 (M.M.-C.). We thank N. van Hulst and C. Genes for helpful discussions and comments. Part of the numerical simulations were performed with the open-source framework QuantumOptics.jl [27].

M.M.-C. and D.P. contributed equally to this work.

[1] R. Lehmberg, Phys. Rev. A **2**, 883 (1970).
[2] M. Gross and S. Haroche, Phys. Rep. **93**, 301 (1982).
[3] H. Zoubi and H. Ritsch, Europhysics Letters **82**, 14001 (2008).
[4] S. D. Jenkins, J. Ruostekoski, N. Papasimakis, S. Savo, and N. I. Zheludev, Phys. Rev. Lett. **119**, 053901 (2017).
[5] M. O. Scully, Phys. Rev. Lett. **102**, 143601 (2009).
[6] H. Zoubi and H. Ritsch, Eur. Phys. J. D **66**, 292 (2012).
[7] L. Ostermann, H. Zoubi, and H. Ritsch, Opt. Express **20**, 29634 (2012).
[8] D. Plankensteiner, L. Ostermann, H. Ritsch, and C. Genes, Sci. Rep. **5**, 16231 (2015).
[9] H. Zoubi and H. Ritsch, Europhysics Letters **90**, 23001 (2010).
[10] A. Asenjo-Garcia, M. Moreno-Cardoner, A. Albrecht, H. J. Kimble, and D. E. Chang, Phys. Rev. X **7**, 031024 (2017).
[11] H. Zoubi and H. Ritsch, New J. Phys. **12**, 103014 (2010).
[12] L. Ostermann, C. Meignant, C. Genes, and H. Ritsch, New J. Phys. **21**, 025004 (2019).
[13] Y.-X. Zhang and K. Mølmer, Phys. Rev. Lett. **122**, 203605 (2019).
[14] J. Ruostekoski and J. Javanainen, Phys. Rev. A **96**, 033857 (2017).
[15] M. L. Brongersma, J. W. Hartman, and H. A. Atwater, Phys. Rev. B **62**, R16356 (2000).
[16] A. Serafini, S. Mancini, and S. Bose, Phys. Rev. Lett. **96**, 010503 (2006).
[17] R. E. Blankenship, *Molecular Mechanisms of Photosynthesis* (Wiley, New York, 2014).
[18] N. Nelson and A. Ben-Shem, Nat. Rev. Mol. Cell Biol. **6**, 818 (2005).
[19] R. J. Cogdell, A. Gall, and J. Köhler, Q. Rev. Biophys. **39**, 227 (2006).
[20] W. M. Brown and E. M. Gauger, J. Phys. Chem. Lett. **10**, 4323 (2019).
[21] G. S. Engel, T. R. Calhoun, E. L. Read, T. Ahn, T. Manal, Y.-C. Cheng, R. E. Blankenship, and G. R. Fleming, Nature (London) **446**, 782 (2007).
[22] G. Panitchayangkoon, D. V. Voronine, D. Abramavicius, J. R. Caram, N. H. C. Lewis, S. Mukamel, and G. S. Engel, Proc. Natl. Acad. Sci. USA **108**, 20908 (2011).
[23] A. Asenjo-Garcia, J. D. Hood, D. E. Chang, and H. J. Kimble, Phys. Rev. A **95**, 033818 (2017).
[24] R. H. Dicke, Phys. Rev. **93**, 99 (1954).
[25] M. Hebenstreit, B. Kraus, L. Ostermann, and H. Ritsch, Phys. Rev. Lett. **118**, 143602 (2017).
[26] P. O. Guimond, A. Grankin, D. V. Vasilyev, B. Vermersch, and P. Zoller, Phys. Rev. Lett. **122**, 093601 (2019).
[27] S. Krämer, D. Plankensteiner, L. Ostermann, and H. Ritsch, Comput. Phys. Commun. **227**, 109 (2018).